MULTIRESOLUTION RECONSTRUCTION OF LOCAL DROP-SIZE DISTRIBUTIONS AND LIQUID VOLUME CONCENTRATION FROM FINITE-WIDTH LASER DIFFRACTION DATA

Songrit Tanchatchawan, Pumyos Vallikul, Pisit Yongyingsakthavorn, Christophe Dumouchel

MULTI-RESOLUTION RECONSTRUCTION OF LOCAL DROP-SIZE DISTRIBUTION AND LIQUID VOLUME CONCENTRATION FROM A FINITE-WIDTH LASER DIFFRACTION DATA

Songrit TANCHATCHAWAN[1,2]*, Pumyos VALLIKUL[1],
Pisit YONGYINGSAKTHAVORN[1], Christophe DUMOUCHEL[3]

[1]Department of Mechanical and Aerospace Engineering, Faculty of Engineering,
King Mongkut's University of Technology North Bangkok, Thailand
[2]Engineering Department, Thailand Institute of Scientific and Technological Research
[3]CORIA – UMR 6614, Normandie Université, CNRS, Université et INSA de Rouen, France
* Corresponding author: songrit@tistr.or.th

ABSTRACT

This paper introduces a multi-resolution tomographic algorithm to reconstruct drop-size distribution and liquid volume concentration within local regions of sprays. The reconstruction procedures allow the size of the local regions to be designated adaptively such that the reconstruction results can be obtained at multiple resolutions. The algorithm employs the strip integration together with laser diffraction measurements with overlapping beam sampling. The algorithm has been tested with both the synthetic and measured line-of-sight data of a solid cone spray. The reconstructed results from this algorithm are in the form of local volume-weighted drop-size distributions which contain both qualitative and quantitative information of the drop-size distribution. The reconstruction results are comparable to those obtained by using the classical reconstruction technique with a smaller laser beam diameter. The comparison shows good agreement, however, the proposed measurement technique consumed less calculation time and spent less working hour on measurement setup procedures.

Keywords: multi-resolution tomographic algorithm, volume-weighted drop-size distribution, laser diffraction

1. INTRODUCTION

Spray characterization is very important for many purposes. For instance, in combustion, liquid fuel is needed to be atomized in small drops before burning. The increase of the total drop-interface area promotes mass and heat transfer and lead to a better mixing, an easier igniting, and a smaller drop burning time. Furthermore, smaller fuel drops lead to higher heat release rates and lower concentrations of pollutant emissions (Lefebvre, A. H. (1985) and Rink, K. K. and Lefebvre, A. H. (1986)). Several methods to measure spray drop-size distributions have been developed: drop collection on slides, high–speed photography, hot-wire technique, Phase Doppler Particle Analysis (PDPA), Laser Diffraction Technique (LDT) (McCreath, C. G. and Beer, J. M. (1976), Jones, A. R. (1977), Chigier, N. A. (1983) and Lefebvre, A. H. (1989)). Being based on the interaction between the liquid drop and laser light, the latter two are the most popular. The information they report is fundamentally different and this for two reasons. First, the PDPA performs a temporal spray sampling whereas the LDT performs a spatial sampling. Dodge et al. (1987) demonstrated that this difference prohibits the direct comparisons between PDPA and LDT drop-diameter distributions unless appropriate precautions are taken. Second, whereas the PDPA reports spatially localized information, the LDT produces a line-of-sight (or spatially integrated) drop diameter distribution. In many situations, this spatially integrated characteristic could constitute a drawback of the LDT. In order to overcome this drawback, deconvolution techniques (or tomographic reconstruction) have been developed in the literature to recover local information from LDT measurements. The present paper intends to contribute to the improvement of these techniques.

The LDT principle rests on the recording on a series of concentric diodes of the forward scattered intensity pattern due to the interaction between a spray and a laser beam. Developed for axisymmetric sprays only, the deconvolution techniques consists in

performing a series of measurements by shifting the LDT laser beam in order to probe the whole spray. This series of spatially integrated information is then related to local information, producing a system of equations that has to be solved to retrieve local drop-size distribution. In the early deconvolution techniques, the system of equations was solved with the Abel transformation or onion peeling method (Hammond (1981), Yule et al. (1981), Dodge et al. (1987), Drallmeier and Peters (1994), Lee and Reitz (2004)) Resolving the equations one after the other, the onion peeling method is known to accumulate the error while the resolution proceeds. In the context of drop-diameter distribution deconvolution, this results in a rather inaccurate distribution in the spray central regions. To overcome the drawback of the onion peeling method, Yongyingsakthavorn et al. (2007, 2009) developed the Maximum Entropy tomographic reconstruction in which all equations are solved at the same time avoiding the problem of inaccuracy concentration. This technique was successfully applied to determine local spray drop-size distributions (Yongyingsakthavorn et al. 2007) and local volume concentrations (Yongyingsakthavorn et al. 2009). However, a lack of spatial resolution was prominently disclosed by comparing the line-of-sight distribution with the one obtained from the spatial integration of the local drop-size distributions.

The spatial resolution of the deconvolution technique is imposed by the width and by the lateral shift of the laser beam when producing the series of measurements probing the whole spray. In the previous studies mentioned above, the radial shift was always equal to the diameter of the laser beam. In this condition the number of unknowns to be determined by the deconvolution procedure is exactly equal to the number of equations in the system. The problem is therefore correctly closed. The increase of the spatial resolution can be achieved either by reducing the diameter of the laser beam or by reducing the radial shift of the laser-beam allowing the overlapping of successive measurements. The second method was developed by Boyaval and Dumouchel (2001). They made the radial shift equal to the radius

of the laser beam, the problem remained solvable and an improved spatial resolution can be obtained. The drawback of this technique is the increase of the number of unknowns of the problem while the radial shift decreases. To remedy this, the number of the unknowns has to be delimited, at a solvable number, and the unknowns should be constructed independently from both the lateral shifting and the width of the probing laser beam.

In this work, we proposed a multi-resolution reconstruction algorithm to reconstruct volume-weight drop-size distribution of liquid droplets within a solid cone spray. With this technique, the domain of the reconstruction problem is in the form of local region pattern (LRP). The LRP is a priori defined and is independent from the line-of-sight sampling scheme. Furthermore it can have multiple resolutions: At the outer skirt of a solid cone spray where the spatial dependency of drop-size-distributions is weak, the LRP is designed to have low resolution. Other places where the characteristics of the drop-size-distribution depend strongly on the radial position, the LRP is of high resolution pattern. The idea has been advanced from a previous work (Tanchatchawan et al., 2013a) where the multi-resolution reconstruction techniques had been used to measure and characterize a flat spray.

The outline of this paper is the following. Section 2, redefines the scattered and the extinction strip integration models and the volume-weighted drop-size distribution used to characterize the liquid sprays. Section 3 shows the construction of strip integration data from a mathematical function which simulates an axisymetrical spray. Using this noise free strip integration data, the proposed reconstruction algorithm has been applied to reconstruct the original mathematical function. The reconstruction has been performed on the predefined multi-resolution LRPs. Section 4 applies the multi-resolution reconstruction technique to reconstruct a solid cone water spray from the strip integration data obtained from the line-of-sight measurement. This section also shows the reconstruction results of the same spray when

using a reduced size probe laser beam measurement data and the results are used to validate with that obtained from the proposed adaptive reconstruction methods.

2. STRIP-INGRATION MODELS FOR SCATTERED AND TRANSMITTED LIGHT INTENSITIES

2.1 The strip-integration models of local intensity and extinction coefficient

Models of scattered and transmitted light intensities from a line-of-sight laser beam passing through a spray of non-homogeneous drop-size-distributions are constructed in this section. Let us consider a cloud of droplets of an axisymmetric spray. When a laser beam passes through this cloud along the path of length *S*, the light is scattered and attenuated (see Fig. 1). At each point (*s*, *w*) we introduce the local intensity $I_\theta(s,w)$ scattered at angle θ and the local extinction coefficient $k(s,w)$. The resulting intensity scattering at angle θ is the sum of the contribution of each point, i.e.:

$$\bar{I}_\theta = \int_0^S \int_0^W I_\theta(s,w)dw\,ds \tag{1}$$

The line-of-sight extinction intensity follows the Beer-Lambert law as:

$$I_L = I_0 exp\left(-\int_0^S \bar{K}_W(s)\,ds\right). \tag{2}$$

The integrand $\bar{K}_W(s)$ in Eq. (2) is the average local extinction coefficient over the width W of the laser beam, i.e.:

$$\bar{K}_W(s) = \frac{1}{W}\int_0^W k(s,w)dw. \tag{3}$$

Equations (2) and (3) can be rearranged as:

$$I_L = I_0 exp\left(-\frac{1}{W}\int_0^S \int_0^W k(s,w)dw\,ds\right) \tag{4}$$

Equations (1) and (4), are called the strip integration models since they integrate the changes over the plane area ($S \times W$) of the laser beam. As can be seen from the Figure 1, the values of the strip integration intensities $\bar{I}_\theta$ and I_L are those given by LDT measurements. Equations (1) and (4) form the scattered and extinction tomographic problems whose unknowns are the local scattered intensity I_θ and the local extinction coefficient k, respectively. The algorithm to solve the tomographic problems using the computer simulated strip-integration function is introduced in the next section.

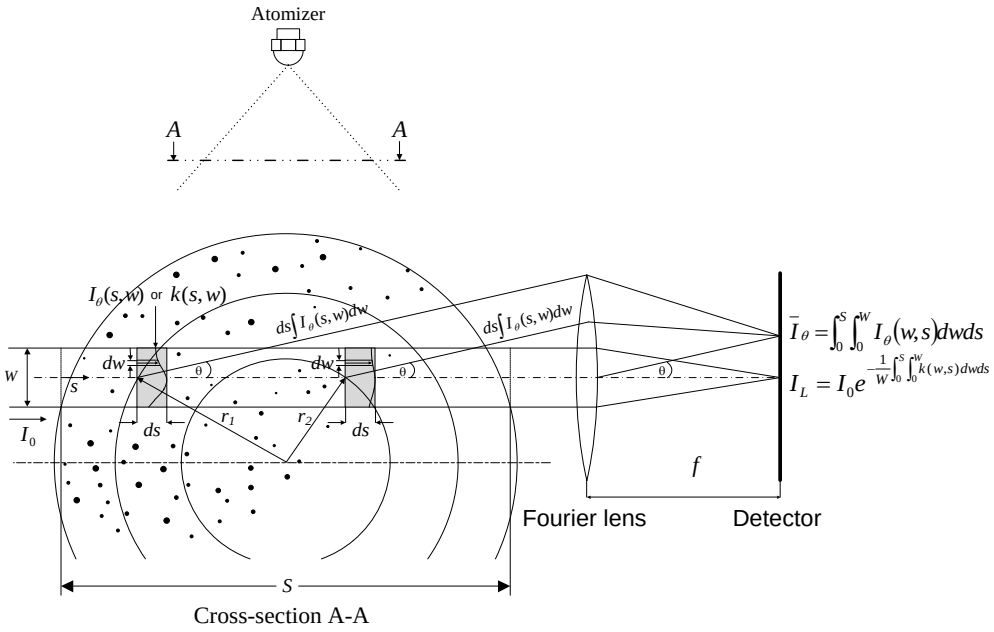

Figure 1 Light scattering diagram of laser beam passing through spray

2.2 Volume-weighted drop-size distribution

The reconstructed local scattered intensities I_θ can provide local volume-based drop diameter distribution , $f_v(D)$ (Mayer and Chigier (1986)) and from which the local Sauter mean diameter, D_{32} can be determined:

$$D_{32} = \frac{\int_0^\infty f_v(D)dD}{\int_0^\infty f_v(D)D^{-1}dD} \tag{5}$$

The reconstructed average local extinction coefficient, $\overline{K}$, together with D_{32} can be used to determine the local liquid volume concentration, C_v, (Yongyingsakthavorn et al. 2009):

$$C_v = \frac{2D_{32}\overline{K}}{3\bar{Q}} \tag{6}$$

Where $\bar{Q}$ is the mean scattering coefficient whose value is a function of D_{32} and of the liquid refractive index (Dobbins and Jizmagian, 1966).

The local liquid volume; i.e. the liquid contained in all droplets of the local region, can be calculated by:

$$V = C_v V_m \tag{7}$$

where V_m is the local measurement volume

The local liquid volume V, is a quantitative local information complementary to the local drop-diameter distribution, $f_v(D)$, which is a qualitative local information. The product of these two pieces of information is the local volume-weighted drop-diameter distribution (Yongyingsakthavorn et al., 2009, 2011) and the area delimited by this new distribution represents the liquid volume of the droplets. In consequence, the volume-weight drop-diameter distributions of two adjacent regions can be added up and the area under the new distributions would be the total liquid volume of the two regions. Conversely, the volume based drop-diameter distribution $f_v(D)$ of combined regions is simply the volume-weighted drop-diameter distribution of the combined regions divided by the area delimited by this distribution. This can be mathematically expressed

$$f_v(D_i) = \frac{\sum_{j=1}^{N} f_{v,j}(D_i)V_j}{\sum_{i=1}^{m}\left[\Delta D_i\left(\sum_{j=1}^{N} f_{v,j}(D_i)V_j\right)\right]}. \tag{8}$$

Where *N* is the number of adjacent regions and m the number of diameter classes.

3. RECONSTRUCTION FROM SYNTHETIC TOMOGRAPHIC DATA

In this section, we use a mathematical function (called a true function) to represent local information . From this function, the exact strip integration function is analytically constructed and used to test the reconstruction algorithm. At the end of the section, the reconstruction problems are formulated using the same strip integration function but with different LRPs. The problems are then solved using the maximum entropy technique.

3.1 Synthesis of strip integration from a mathematical function

The mathematical (or the true) function is an axisymmetric function defined by:

$$f(r) = \begin{cases} 0.25, & 0 \le r \le 2.5 \\ 1.00, & 2.5 < r \le 5.0 \\ 0.50, & 5.0 < r \le 10 \\ 0.00, & r > 10 \end{cases} . \tag{9}$$

The rotation and the half-plane one dimensional plots of the function are shown in Figure 2. Since the function $f(x, y)$ is known, the strip integration function $P(y)$ along the y axis can be exactly calculated. It comes:

$$P(y) = \int_0^S \int_{y-\frac{W}{2}}^{y+\frac{W}{2}} f(x,y)dy\,dx\,. \tag{10}$$

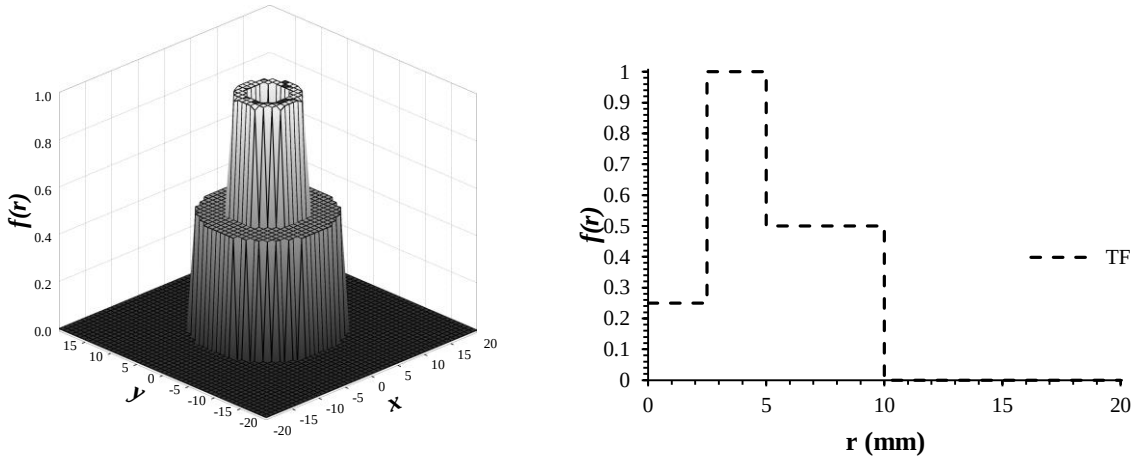

Figure 2 The rotation and one dimensional plot of the true function

If $P(y)$ is known for four discrete strips, the strip integration Eq. (10) can be written as:

$$\begin{Bmatrix} P_1 \\ P_2 \\ P_3 \\ P_4 \end{Bmatrix} = \begin{bmatrix} a_{11} & a_{12} & a_{13} \\ a_{21} & a_{22} & a_{23} \\ a_{31} & a_{32} & a_{33} \\ a_{41} & a_{42} & a_{43} \end{bmatrix} \begin{Bmatrix} f_1 \\ f_2 \\ f_3 \end{Bmatrix}. \tag{11}$$

f_1, f_2 and f_3 correspond to the three local value of the true function *f(r)* (Eq. (9)). The element a_{ij} represents the intersection area between the strip i and the region j. This matrix is called the characteristic matrix of the true function. As an illustration, we consider four strips located at y_i = 12.5, 10, 7.5 and 5 mm and a strip width equal to 10 mm (see Figure 3). According to Eq. (10), the numerical values of the characteristic matrix can be determined. We obtained:

$$\begin{Bmatrix} P_1 \\ P_2 \\ P_3 \\ P_4 \end{Bmatrix} = \begin{bmatrix} 0.2267 & 0.0000 & 0.0000 \\ 0.6142 & 0.0000 & 0.0000 \\ 0.9225 & 0.1535 & 0.0000 \\ 1.1781 & 0.2945 & 0.0982 \end{bmatrix} \begin{Bmatrix} 0.5 \\ 1 \\ 0.25 \end{Bmatrix} = \begin{Bmatrix} 0.1134 \\ 0.3071 \\ 0.6148 \\ 0.9081 \end{Bmatrix}, \tag{12}$$

The projection function and the measurement projection corresponding to Eq. (12) are shown in Fig. 3. The characteristic matrix in Eq. (12) of the true function tells that the fourth strip passes all the three local regions, the third strip passes only two local regions and the first two strips pass the outer most local region only.

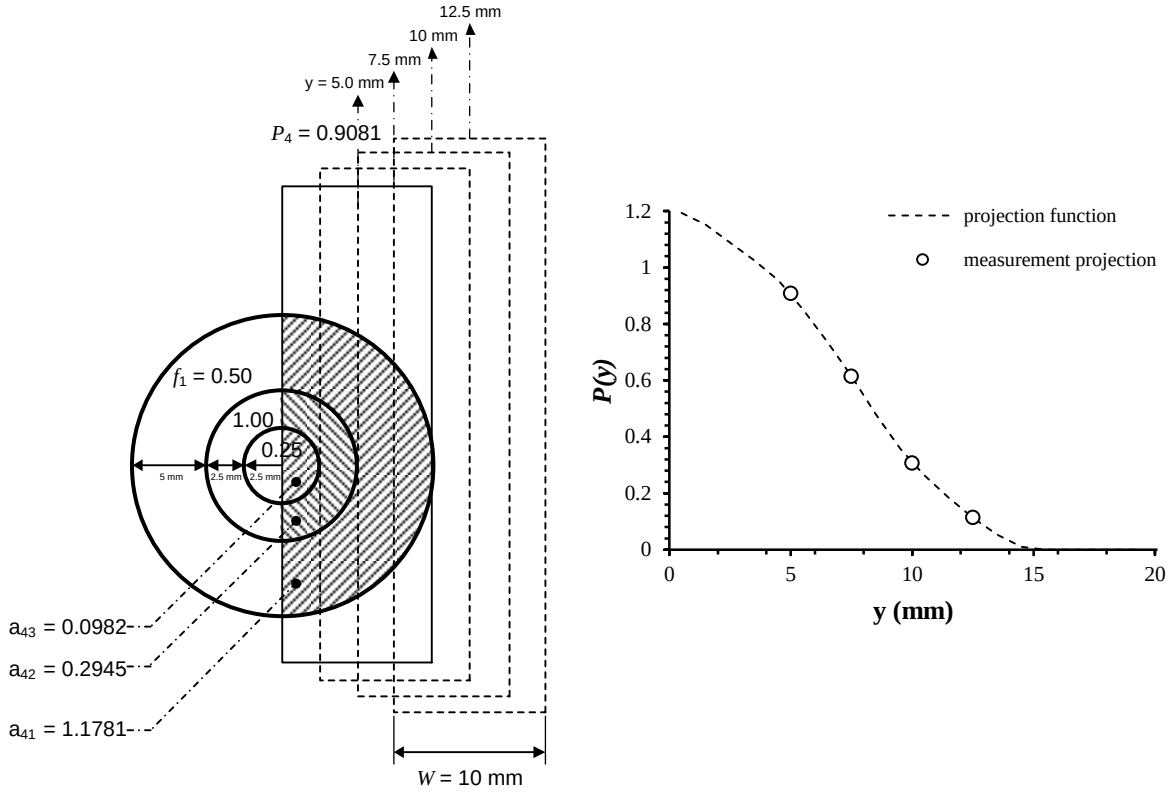

Figure 3 The rotation and one dimensional plot of the true function.

3.2 Reconstructions from the synthetic strip integration data

The resulting strip integration, $[P_1 \quad P_2 \quad P_3 \quad P_4]$, are now used as line-of-sight measurement data to reconstruct local functions of different patterns. The effect of the local region patterns on the reconstruction results is considered by using three Local Region Pattern (LRP). The three LRPs are shown in Figure 4 (left). The 1st LRP has only a single central region whose radius is equal to 10 mm. The local value f_1 of this unique region is to be reconstructed. The four strips pass the local region, each of them intersecting the local region at different position. The intersected areas are calculated and constitute the characteristic matrix of the 1st LRP. The reconstruction problem can then be written numerically as:

$$\begin{bmatrix} 0.2267 \\ 0.6142 \\ 1.0760 \\ 1.5708 \end{bmatrix} f_1 = \begin{Bmatrix} 0.1134 \\ 0.3071 \\ 0.6148 \\ 0.9081 \end{Bmatrix}. \quad (13)$$

The problem is over determined and has been solved using the maximum entropy technique. The solution to the problem is plotted in comparison with the true function and shown in the top row of Figure 4 (right). As expected, the 1st LRP needs refinement in order to obtain a better reconstruction solution.

The 2nd LRP has one inner region of 5 mm radius and one concentric outer region between 5 and 10 mm. The characteristic matric of the 2nd LRP is:

$$\begin{bmatrix} 0.2267 & 0.0000 \\ 0.6142 & 0.0000 \\ 0.9225 & 0.1535 \\ 1.1781 & 0.3927 \end{bmatrix} \begin{Bmatrix} f_1 \\ f_2 \end{Bmatrix} = \begin{Bmatrix} 0.1134 \\ 0.3071 \\ 0.6148 \\ 0.9081 \end{Bmatrix}. \quad (14)$$

The solution of this problem is shown in the middle row of Figure 4 (right). It captures the outer region very well but still requires refinement to correctly catch the inner regions.

The 3rd LRP is designed to have the same shape as the domain of the true function. The reconstruction problem gives:

$$\begin{bmatrix} 0.2267 & 0.0000 & 0.0000 \\ 0.6142 & 0.0000 & 0.0000 \\ 0.9225 & 0.1535 & 0.0000 \\ 1.1781 & 0.2945 & 0.0982 \end{bmatrix} \begin{Bmatrix} f_1 \\ f_2 \\ f_3 \end{Bmatrix} = \begin{Bmatrix} 0.1134 \\ 0.3071 \\ 0.6148 \\ 0.9081 \end{Bmatrix}. \quad (15)$$

The solution to the 3rd LRP problem is the one expected which means that the LRP has a sufficient resolution to resolve the true function. Also the correct solution means that the strip integration functions used contain the information needed for the reconstruction.

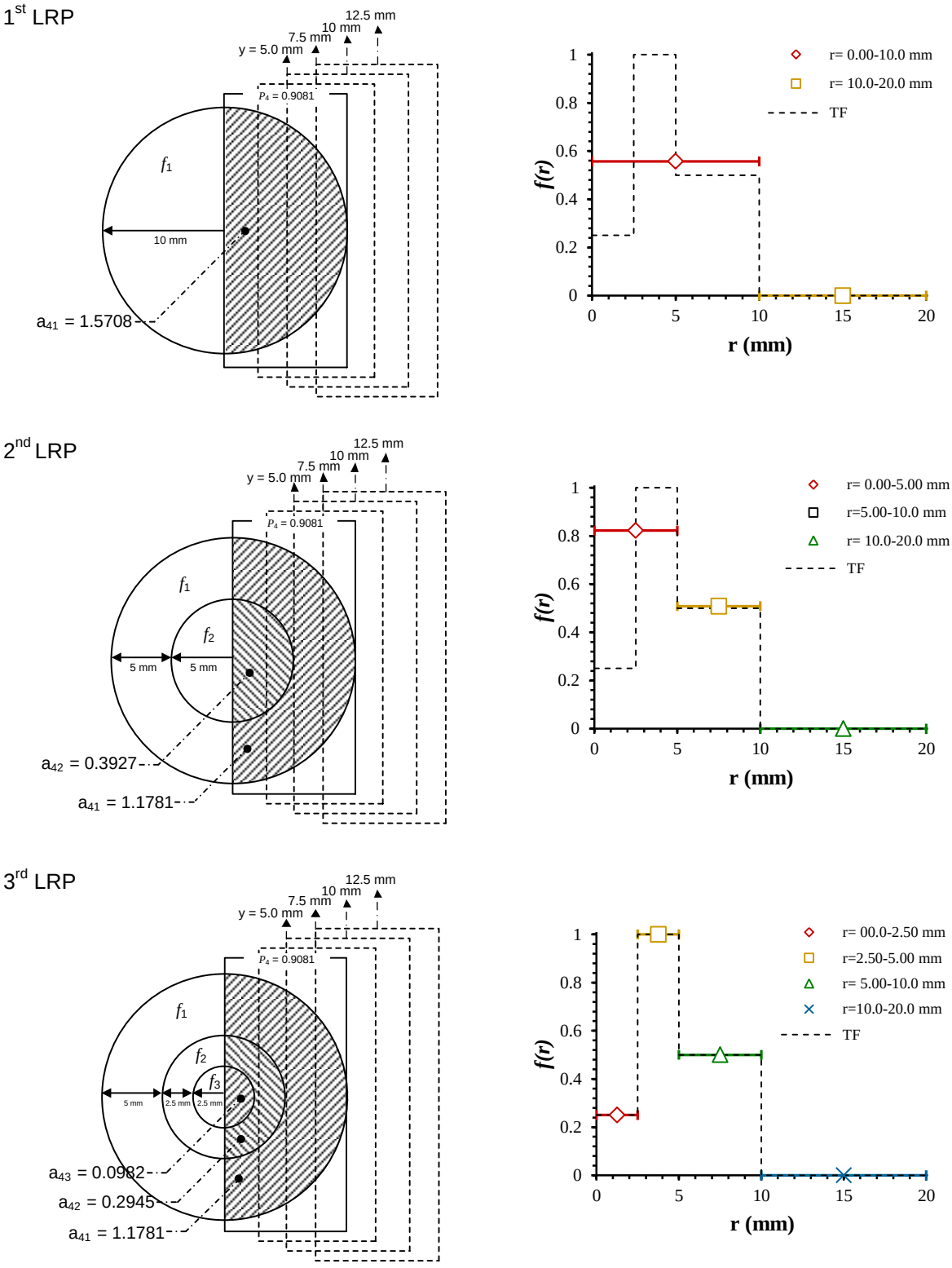

Figure 4 Local region patterns (left) and the reconstruction results (right)

4. RECONSTRUCTED RESULTS OF SOLID-CONE SPRAY

The proposed reconstruction procedure is applied to reconstruct drop-diameter distribution and liquid volume concentration within local regions of a solid cone water-spray. Descriptions of the spray and the measurement procedures are detailed in subsection 4.1. The reconstruction results and verifications are shown in subsection 4.2. We used synthetic strip integration past the center of the spray to verify the reconstruction results. The 10 mm-width synthetic strip is constructed from the measurement results and is compared with the direct measurement of line-of-sight data.

4.1 Measurement series

The liquid spray examined in this work is produced by a swirl atomizer. The injection pressure is equal to 12 bars, corresponding to a mass flow rate equal to 4 kg/hr. The spray is assumed axi-symmetric and is scanned on one half only. Two laser beams are used. They differ by their diameter which is equal to 10 mm and 3.33 mm. Figure 5 shows the schematic diagram of the different scans. With the 10 mm laser beam, the sampling spatial frequency depends on the position *y*. For *y* ranging from 5 mm to 35 mm, the sampling spatial frequency is equal to $\frac{1}{2.5}mm^{-1}$ and for *y* beyond 35 mm, it is equal to $\frac{1}{10}mm^{-1}$. There is no beam overlapping when scanning with the smaller laser beam diameter. Therefore, in this case, the sampling spatial frequency is equal to $\frac{1}{3.3}mm^{-1}$. For each experiment, scans end when no interaction between the light and the spray is detected. For the 10 mm and 3.33 mm laser beams, this occurs at *y* = 55 mm and 51.615 mm, respectively.

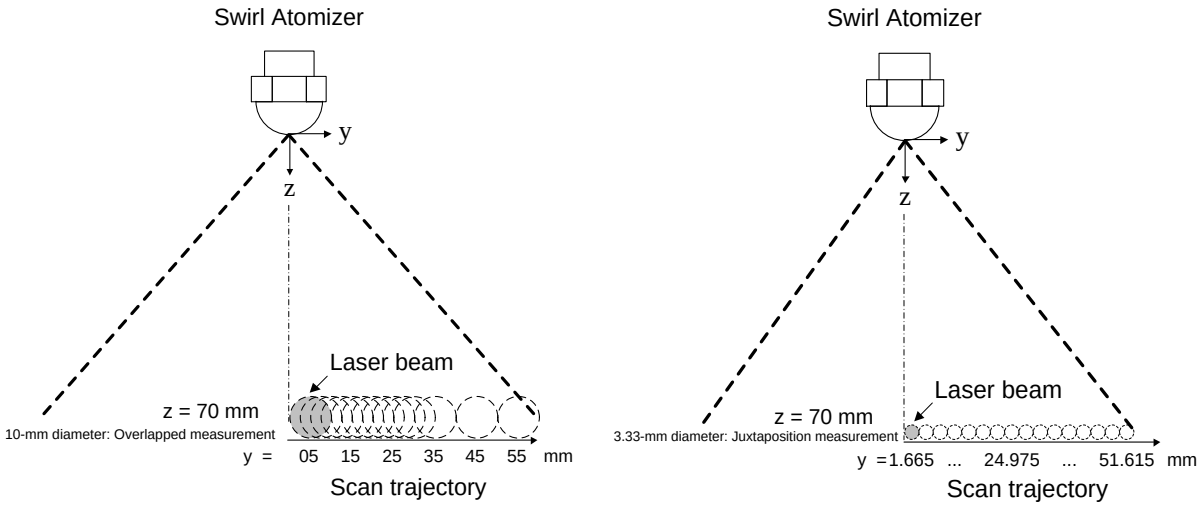

Figure 5 Schematic diagram of the laser beam measurement

4.2 The local region patterns

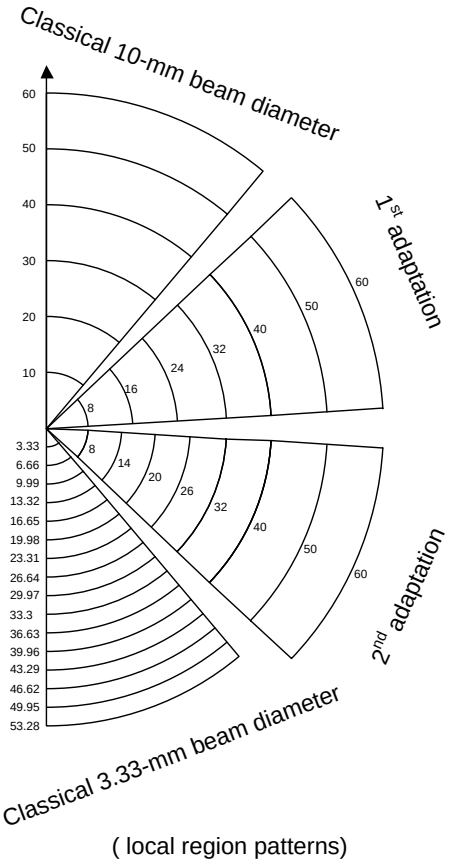

Figure 6 The Four Local Regions Patterns (right) of the solid-cone spray

Figure 6 shows the sections of the four LRPs used to test the reconstruction algorithm. The three firsts (Classical 10, 1st Adaptation and 2nd Adaptation) are constructed for the

measurement series with the 10 mm laser beam. The Classical 10 pattern has all local regions of 10 mm-width and being equal to the diameter of the probing laser beam. The 1st Adaptation pattern has two different widths of local regions. The width of the two outermost rings is equal to 10 mm and the one of the inner rings and of the central region is equal to 8 mm. The 2nd Adaptation pattern involves three different widths of local regions. The width of the central region is equal to 8 mm, the one of the four following inner regions is equal to 6 mm, the width of the sixth region is equal to 8 mm and, finally, the two outer regions have a width to 10 mm. The local region width is reduced for regions where the spatial gradient of the spray drop diameter distribution is expected to be the greatest.

The fourth Local Region pattern (Classical 3.33) corresponds to the measurements series with the small diameter laser beam. In this case, the width of the local regions is equal to the laser beam diameter, i.e., 3.33 mm. More generally, we note that the width of the local regions are always less than or equal to the width of the probe laser beam. As for the lower limit, the width of the local region cannot be smaller than the distance of the smallest radial shift.

4.3 Strip integration model

Figure 7 shows the conceptual drawing and parameters involved in the strip integration model of the solid cone spray. There are N local regions and M strip integrations. The indexes count from the outermost to innermost positions of the measurement plane. The j^{th} local scattered intensity and local extinction coefficient are represented by I_j and k_j, respectively and they are bounded by the outer and inner radii $r_j \; and \; r_{j+1}$, except the N^{th} local region which is at the center core of the spray.

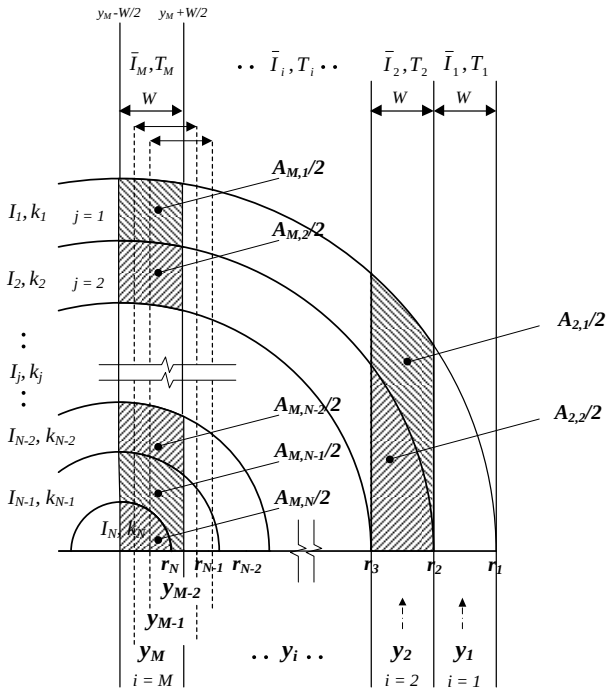

Figure 7 Conceptual drawing shows parameters involved in strip integration for the solid cone spray at different local region pattern

The i^{th} strip integral intensity and transmittances are represented by $\bar{I}_i$ and T_i respectively. The i^{th} strip lays along the line y_i having the width equal to the diameter of the laser beam. The left and the right boundaries of the strip i^{th} are along the lines $y_i - W/2$ and $y_i + W/2$, respectively. Figure 7 also introduces the internal areas $A_{i,j}$ that are defined as the intersection area between the j^{th} local region positioned at $(r_j + r_{j+1})/2$ and the i^{th} strip positioned at y_i. The strip integration model for the solid-cone spray measurement writes:

$$\bar{I}_i = \sum_{j=1}^{N} A_{i,j}\, I_j \tag{15}$$

$A_{i,j}$ represents the contribution of sub-region j on measurement i. If measurement i does not intercept sub-region j, then the corresponding A_{ij} is set to 0.

Furthermore the relationship between strip integrated transmittance, T_i and the local extinction coefficient, k_j is given by:

$$-\ln T_i\, W \;=\; \sum_{j=1}^{N} A_{i,j}\, k_j \tag{16}$$

The values A_{ij} are similar to those defined in the strip integration and W is the width of the laser beam. The calculation of A_{ij} is shown in the Appendix at the end of the paper.

4.4 Verification and validation

For verification purposes, the 10 mm-width synthetic strip integration that passes the center of the spray is constructed only (See Fig. 8). The synthetic strips integration is constructed for the four local region patterns defined in Fig. 6.

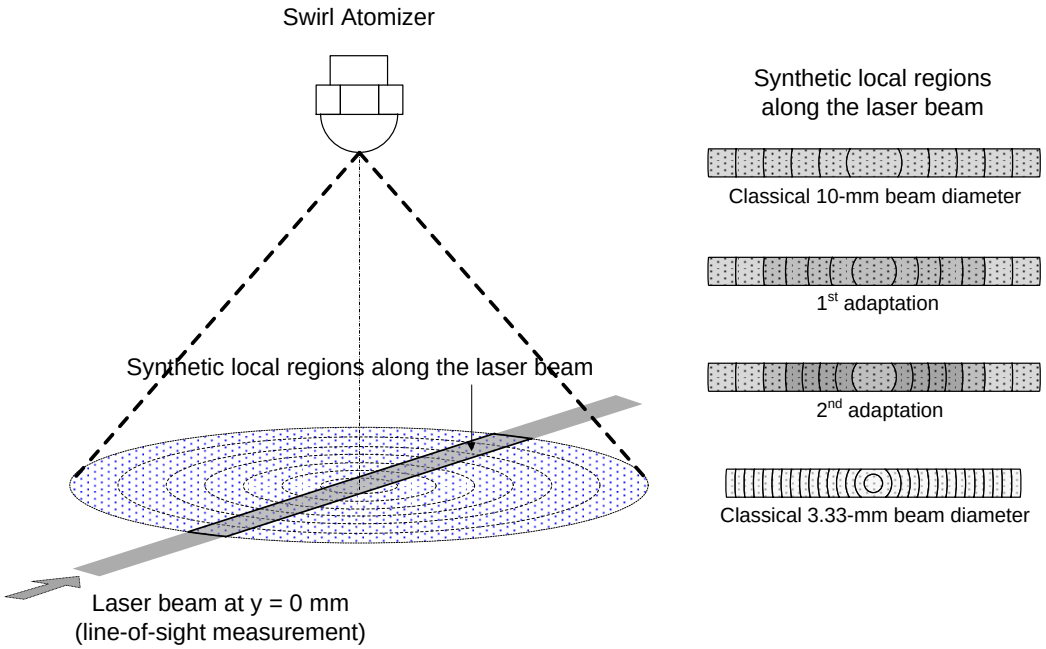

FIGURE 8 Concentric ring regions and weighted volumes along the laser beam

Figure 9 shows the local and the combined volume-weighted drop-size distributions along the line-of-sight for the four LRPs. The top row shows reconstruction for the Classical 10 mm LRP and the 1st Adaptation LRP. As expected, the local distributions obtained from

these two LRPs report that the spray contains less and less big drops when going towards the center. The local distributions can be combined into a global volume-weight drop-size distributions (see section 2.2). The combined distributions show oscillations in the inner regions. However, these oscillations are less pronounced for the more LRP, i.e., for the 1st Adaptation one.

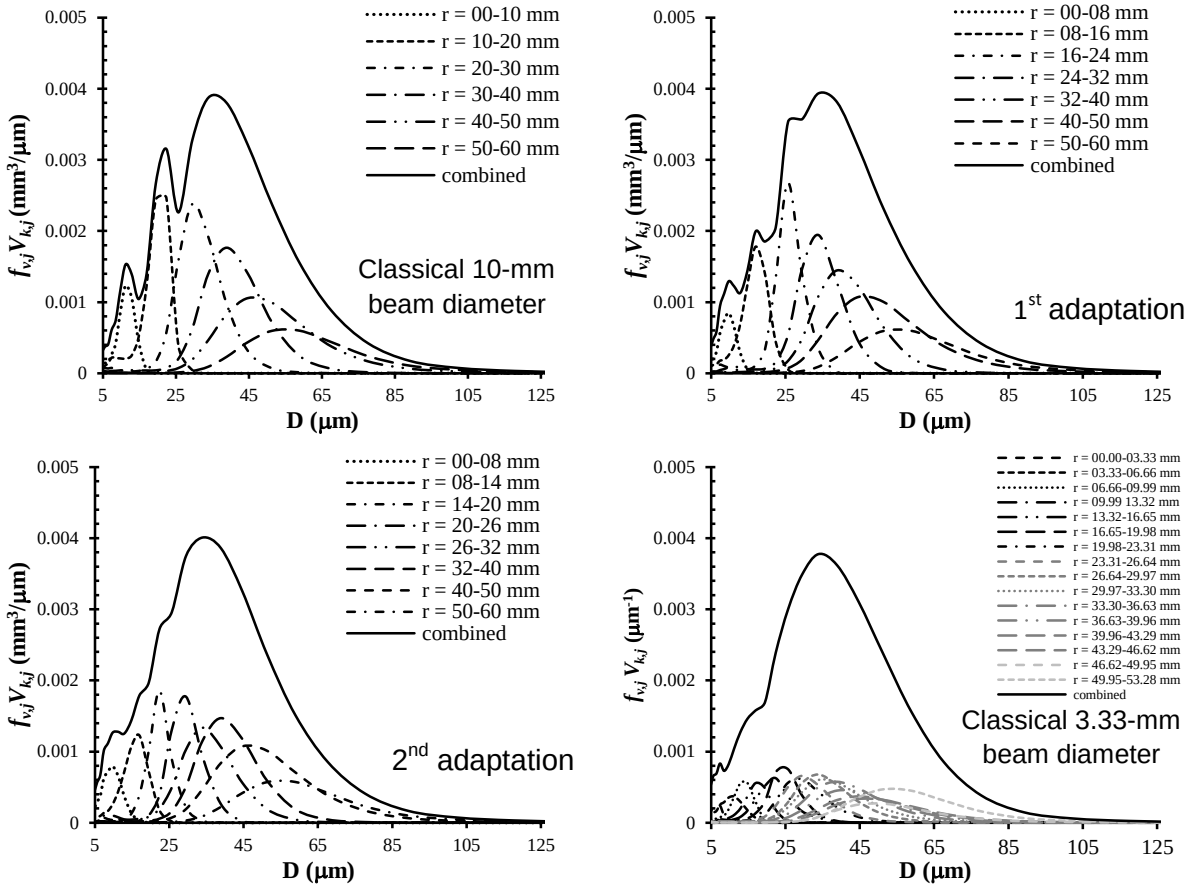

Figure 9 Volume-weighted distributions of local volume and combined regions at different local region pattern

Reconstruction results for the 2nd Adaptation LRP and the Classical 3.33 mm LRP are shown in the lower row of Figure 9. We note that the 2nd Adaptation LRP reveals a combined distribution with even oscillation than for the 1st Adaptation situation. This indicates that the refinement provided by the 2nd Adaptation LRP is both relevant and necessary. Furthermore,

we note that the combined distribution obtained with this LRP agrees closely with the one provided by the Classical 3.3 mm LRP.

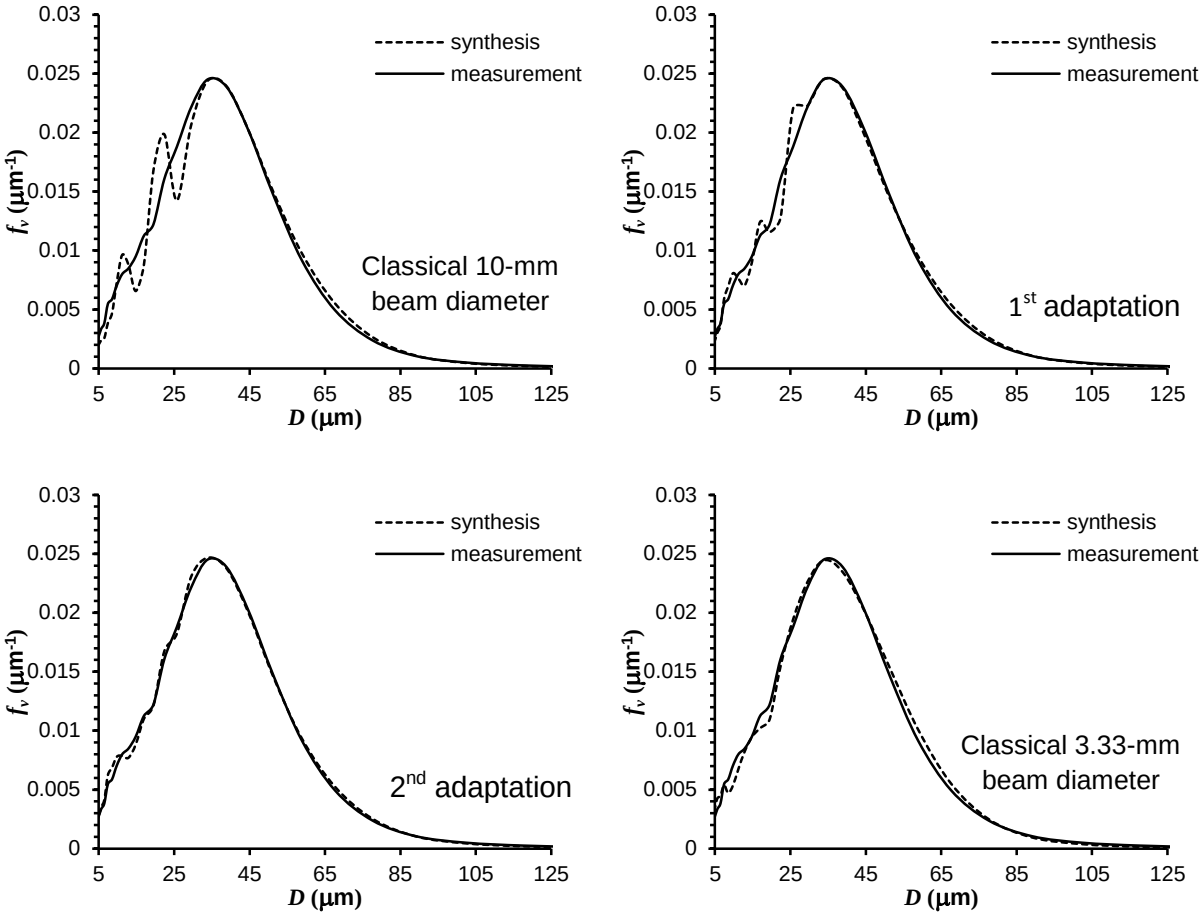

Figure 10 Comparison between the line-of-sight measured volume-based diameter distributions at y = 0 with the combined distributions obtained from the local-distributions for the four LRPs

Figure 10 shows the integrated volume-based diameter distribution at the position $y = 0$. The continuous line is the distribution obtained from a classical line-of-sight measurement. The dash line (synthesis) corresponds to a combined distribution obtained from the local distributions according to Eq. (7). Each graph shows the combined distribution obtained for a specific LRP. When comparing the synthesis and measured line-of-sight drop-size distributions we see that they all report the same distribution in the large diameter region (above 40 µm). For the smaller drops, which are mostly located in the the inner regions of the

spray (see Fig. 9), the synthesis distribution does not well represent the measured line-of-sight drop-size distributions for the two first LRPs. However as noted above, the oscillation almost disappeared with the 2nd Adaptation LRP and the synthesis and measured distributions are very much alike. This confirms that the local regions used for the reconstruction are small enough to resolve the changes within the inner region (y = 0-40mm) of the spray. It also says that the right amount of liquid volume is used to normalize the combined volume-weighted drop-size distribution. It can be seen also from Figure 10 lower-right row that the synthetic drop-size distribution from the reconstruction using 3.33 mm beam does not shows oscillatory behavior and gives similar results as the measured drop-size distribution using 10 mm beam diameter. Reconstruction with the adaptive scheme using large diameter beam shows the competitive results to those obtained from the reconstruction with the laborious measurement using small diameter beam.

5. CONCLUSIONS

The concept of strip integration together with laser diffraction measurements using overlapping beam sampling have been used to retrieve high spatial resolution drop-diameter distributions within a solid-cone liquid spray. It has been shown that the local measurement regions can be made smaller than the width of the laser beam, or, in other words, the inhomogeneity due to widths less than the laser beam diameter can be resolved by the proposed technique.

The reconstruction results produce local drop-diameter distributions and local liquid volume concentrations. These two pieces of information can be combined and represented in the form of volume-weighted drop-diameter distribution. This representation allows one to synthesize line-of-sight drop-size distribution which can then be used to verify the correctness of the reconstruction results and to identify the required spatial refinement to

obtain higher resolution reconstruction. This is the main advantages of the proposed technique over the conventional technique that gives only single resolution reconstruction.

The resolution of the reconstruction results can also be improved by using small diameter probing laser. It has been shown that the reconstructed results have the same quality to those using the adaptive tomographic algorithm with larger laser beam. Measurement with the smaller laser beams, however, needs more laborious measurement work load than those measuring with larger beam diameters.

6. ACKNOWLEDGEMENTS

The first author is being supported under the PhD scholarship program by the Ministry of Sciences and Technology (MOST), Thailand and Thailand Institute of Scientific and Technological Research (TISTR). Research facilities are partially provided by the Joint Graduate School of Energy and Environment, King Mongkut's University of Technology Thonburi and the Graduate School, King Mongkut's University of Technology North Bangkok.

7. REFERENCES

Bevensee, R. M., *Maximum Entropy Solutions to Scientific Problems*, Engleeood Cliffs: Prentice-Hall, 1993.

Boyaval, S. and Dumouchel, C., Deconvolution Technique to Determine Local Spray Drop Size Distributions – Application to High-Pressure Swirl Atomizers, *ILASS-Europe 2001*, Zurich, 2001.

Chigier, N. A., Drop size and velocity Instrumentation, *Prog. Energy Combust. Sci.*, vol.**9**, pp. 155-177, 1983.

Drallmeier, J.A. and Peters, J.E., Liquid- and Vapor-Phase Dynamics of A Solid-Cone Pressure Swirl Atomizer, *Atomization and Sprays*, vol.**4**, pp.135-158, 1994.

Dobbins, R. A. and Jizmagian, G.S., Optical Scattering Cross Sections for Polydispersions of Dielectric Spheres, *The Optical Society of America*, Vol. **56**, pp. 1345-1350, 1966.

Dodge, L.G., Rhodes, D.J. and Reitz R.D., Drop-Size Measurement Techniques for Sprays: Comparison of Malvern Laser-Diffraction and Aeromatrics Phase/Doppler, *Applied Optics*, vol.**26**, no.11, pp.2144-2154, 1987.

Dumouchel, C., Cousin, J., and Triballier, K., On the Role of the Liquid Flow Characteristics on Low-Weber-Number Atomization Processes, *Experiments in Fluids*, vol.**38**, pp.637-647, 2005.

Hammand, Jr, D. C., Deconvolution Technique for Line-of-Sight Optical Scattering Measurements in Axisymmetric Sprays, *Applied Optics*, vol.**20**, no.3, pp. 493-499, 1981.

Ingle, J. D. J. and Crouch, S. R., *Spectrochemical Analysis*. Prentice-Hall, Englewood Cliffs, NJ, 1988.

Jones, A. R., A review of drop size measurement – The application of techniques to dense fuel sprays, *Prog. Energy Combust. Sci*., vol.**3**, pp. 225-233, 1977.

Lee, K. and Reitz, R. D., Investigation of Spray Characteristics from a Low Pressure Common Rail Injector for Use in a Homogeneous Charge Compression Ignition Engine, *Measurement Science and Technology*, vol.**15**, pp. 509-519, 2004.

Lefebvre, A. H., Fuel effect on gas turbine combustion – Ignition, stability, and combustion efficiency, *ASME J. Eng. Gas Turbines Power*, vol.**107**, pp. 24-37, 1985.

Lefebvre, A. H., *Atomization and Sprays*, Hemisphere Publishing Corp., 1989.

Malvern/INSECTEC: EPCS Technical Specification Revision 12.1.98.2.

McCreath, C. G. and Beer, J. M., A review of drop size measurement in fuel sprays, *Applied Energy*, vol.**2**, pp. 3-15, 1976.

Mayer, P. and Chigier, N., Dropsize measurement using Malvern 2200 particle sizer, *Atomization and Spray*, vol. **2**, pp. 261-298, 1986.

Rink, K. K. and Lefebvre, A. H., Influence of fuel drop size and combustor operating conditions on pollutant emissions, SAE Technical Paper 861541, 1986.

Tanchatchawan, S., Vallikul, P., Yongyingsakthavorn, P. and Dumouchel, C., An Adaptive Tomographic Technique to Reconstruct Local Drop Size Distribution of Liquid Spray at Multi-Resolution, ILASS Americas, *25th Annual Conference on Liquid Atomization and Spray Systems*, Pittsburgh, PA, 2013a.

Tanchatchawan, S., Vallikul, P., Yongyingsakthavorn, P. and Dumouchel, C., Reconstruction of Local Volume-Weighted Drop-Size Distribution of A Solid Cone Spray Using Adaptive Tomographic Technique, *The 16th Conference of ILASS-Asia*, Nagasaki, Japan, 2013b.

Yongyingsakthavorn, Y., Vallikul, P., Fungtammasan, B., and Dumouchel C., Application of the Maximum Entropy Technique in Tomographic Reconstruction from Laser Diffraction Data Determine Local Spray Drop Size Distribution, *Exp Fluids*, vol. **42**, pp. 471-481, 2007.

Yongyingsakthavorn, P., Dumouchel, C., Vallikul, P. and Fungtammasan, B., Deconvolution with Maximum Entropy Solution to Determine Local Extinction Coefficient and Local Volume Concentration Values from Laser Diffraction Data, *Particle and Particle Systems Characterization*, vol. **26**, pp. 187-198, 2009.

Yongyingsakthavorn P., Vallikul P., Dumouchel C., Fungtammasan B. and Tuntivoranukul K., Prediction of Evaporation Time and Rate of Water Sprays from Their Local Drop-Diameter Distributions and Liquid Volume Concentration, *Atomization and Spray*, vol. **21**, no. 2, pp. 159-165, 2011.

Yule, A.J., Seng, A.H., Felton, C., Ungut, P.G, and Chigier, A., A Laser Tomographic Investigation of Liquid Fuel Sprays, *Eighteenth symposium (international) on combustion*, pp. 1501-1510, 1981.

APPENDIX

Determination of characteristic matrix $A_{i,j}$

As shown in Figure A-1, the internal area $A_{i,j}$ is the intersection area between thej^{th} local regions and the i^{th}strip whose width is equal to the laser beam diameter W .

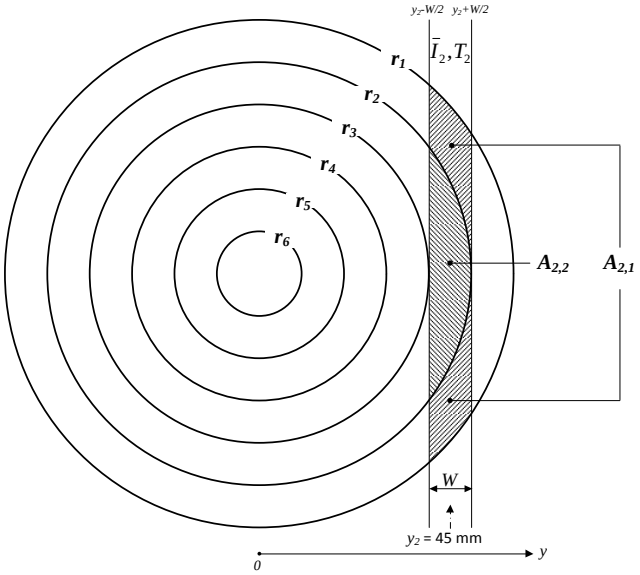

Figure A-1 Example of internal region based on classical LRP with $i = 2$ measurement

The strip integration model for the solid-cone spray measurement is the following

$$\bar{I}_i = \sum_{j=1}^{n} A_{i,j}\, I_j \tag{A1}$$

For any (i, j) pair in Eq. (A1), two parameters are required: n and $A_{i,j}$. The parameter n introduced in Eq. (A1) corresponds to the number of local intensities, $I_1 \ldots I_n$, those contributing to the strip intensity $\bar{I}_i$. The value of n depends on the measurement position yi, the width W and the selected local region pattern. The left edge of the i^{th} strip is the straight

line along the position $y_i - W/2$. The left edge passes through the innermost local region, n^{th}, bounded by the radii r_n and r_{n+1}. Since we consider the case where the width of the local region is equal or less than the width of the laser beamwe have $n \geq j$ only

Before calculating $A_{i,j}$, it is necessary to define the segment S_r^x. The segment is formed by the circle of radius r and the lateral distance x. The segment S_r^x is drawn schematically in Figure A-2 and its mathematical formula is given by Eq. (A2).

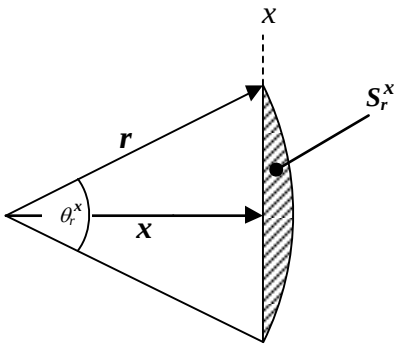

Figure A-2 Definition of the area of segment S_r^x

$$S_r^x = \frac{r^2}{2}\theta_r^x - \sin\theta_r^x \quad \text{where } \theta_r^x = 2\cos^{-1}\left(\frac{x}{r}\right) \text{ in radian} \qquad \text{(A2)}$$

A_{ij} can be defined recursively as

$$\begin{cases} A_{i,j} = S_{r_j}^{y_i - \frac{W}{2}} - S_{r_j}^{y_i + \frac{W}{2}} - \sum_{m=j+1}^{n} A_{i,m} & \text{when } j < n \\ A_{i,j} = S_{r_j}^{y_i - \frac{W}{2}} & \text{when } j = n \end{cases} \qquad \text{(A3)}$$

To illustrate this, we consider the strip $\bar{I}_2$. The left edge of the 2^{nd}strip is the line $y_2 - W/2$. The left edge passes through several local regions where the innermost one is the 2^{nd} region bounded by the radii r_2 and r_3 . Therefore $n = 2$ which means that the local intensity I_1 to I_2 and the internal areas, $A_{2,1}$ to $A_{2,2}$, are involved in the construction of the line of sight intensity $\bar{I}_2$. Namely:

$$\bar{I}_2 = A_{2,1} I_1 + A_{2,2} I_2$$

The internal area $A_{2,1}$ and $A_{2,2}$ can be calculate using Eq. (A3)

$$A_{2,2} = S_{r_2}^{y_2 - \frac{W}{2}}$$

$$A_{2,1} = S_{r_1}^{y_2 - \frac{W}{2}} - S_{r_1}^{y_2 + \frac{W}{2}} - A_{2,2}$$

The schematic of internal area, inner segment and outer segment are shown in Figure A-3

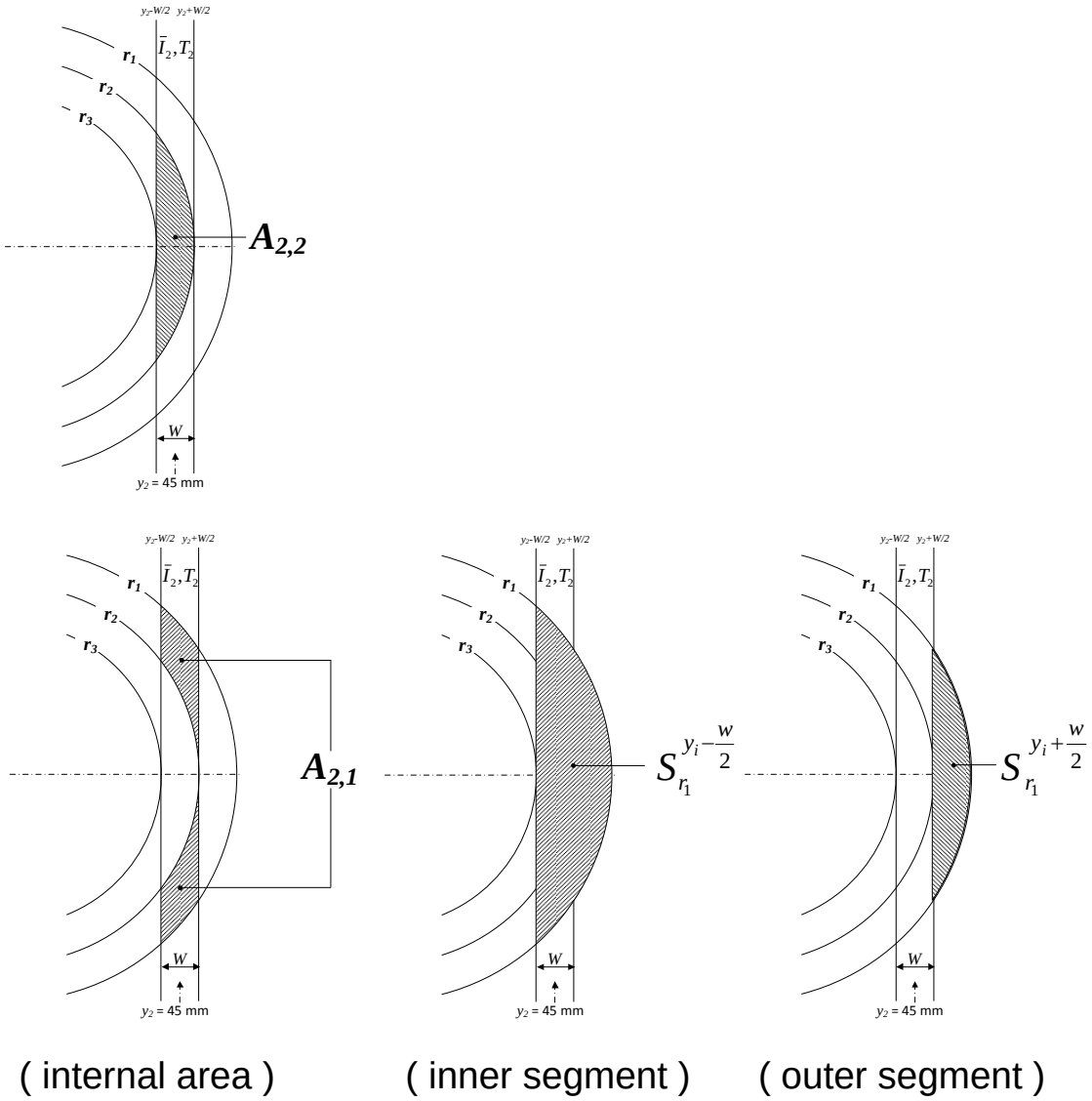

Figure A-3 Schematic of internal area : $A_{2,2}$(top) and $A_{2,1}$(bottom)